Discrete-row growth of xenon adsorbed on the vicinal Pt(997) surface: Comparison between theory and experiment

V. Pouthier, C. Ramseyer, and C. Girardet*
Laboratoire de Physique Moléculaire, UMR-CNRS 6624, Faculté des Sciences La Bouloie, Université de Franche Comté, 25030 Besançon Cedex, France

K. Kuhnke, V. Marsico, M. Blanc, R. Schuster,† and K. Kern
Institut de Physique Expérimentale, Ecole Polytechnique Fédérale de Lausanne, CH-1015 Lausanne, Switzerland
(Received 13 September 1996; revised manuscript received 19 March 1997)

Xe exhibits a discrete-row growth mode on the vicinal Pt(997) surface by sequential attachment to the substrate steps. In order to interpret experimental results obtained by grazing incidence helium scattering, potential calculations are performed. A mean-field Hamiltonian within the two-dimensional Ising model is shown to explain the sequential-row growth observed in helium-atom diffraction studies. More specifically, the calculated temperatures for the occurrence of each row depend mainly on the shape of the potential increment due to the steps and countersteps. They are in good agreement with the experimental values associated with maxima in the scattered He intensity versus coverage curves. [S0163-1829(97)05432-5]

I. INTRODUCTION

Multilayer adsorption has been widely studied[1,2] and the influence of defects[3] has been shown to be important for the wetting/nonwetting transitions that generally occur in adsorbed phases. Indeed, it has been known for a long time that substrate steps are preferential nucleation sites for adsorbates[4,5] due to the increased coordination at step sites. The observation of desorption peaks at increased temperatures and of supplementary ultraviolet photoemission spectroscopy peaks[6,7] for small amounts of adsorbates compared to the monolayer behavior has established step decoration of Xe atoms on vicinal Pt and Pd surfaces. For a sufficiently strong interaction of the adsorbate with an already wetted step a continued attachment of a second row and further rows at the step can be expected. This behavior, which we call discrete-row growth or row-by-row growth, is defined equivalently to layer-by-layer growth. This means that with increasing coverage, the submonolayer film forms a sequence of stable uniform rows with each row being completed before the successive one nucleates. Although its possibility was discussed in literature,[8] this growth mode remained speculative until recently because of the lack of experimental evidence on the one hand and the lack of realistic interaction potentials on the other. A detailed theoretical analysis of row-by-row growth requires the modeling of a real system exhibiting this phenomenon.

Grazing incidence thermal energy helium scattering recently has demonstrated its sensitivity to the order in rows adsorbed at steps. Row completion is observed by maxima in the scattered He intensity. Discrete-row growth was observed for the systems Xe, Ag, and Kr on Pt(997).[9,10] In this paper, we focus on the Xe/Pt(997) system, which is a model system for physisorption. The vicinal surface consists of closed-packed (111) terraces of $\simeq 20$ Å average length separated by monotomic steps. The terrace structure relates this system to the Xe/Pt(111) system, which has been studied in great detail.[11]

The aim of this paper is to model discrete–row-by-row growth using the best available potential form in the literature. We selected the one that appears to be the most appropriate when surface steps are considered for describing the interactions between Xe atoms and the Pt substrate, and the Xe-Xe lateral interactions. Two semianalytical approaches are developed that describe the statistical distribution of the Xe atoms in the adsorption sites of a confined terrace. The ideal lattice-gas model does not take into account the lateral interactions in the adsorbate, but it is expected to give qualitatively the main part of the experimental features. In the mean-field Ising model, the influence of the lateral interactions is considered and it is believed to be accurate enough to interpret the experiments quantitatively. We focus here on the physical process that is involved to favor this row-by-row growth; we thus calculate the mean coverage of a row in terms of a truncated series expansion with respect to the lateral potential in order to keep the analytical simplicity of the model. To get better accuracy would require the use of more accurate potentials and involved numerical methods[8] such as transfer-matrix procedures that would not provide, however, additional fundamental understanding of the growth phenomenon.

II. EXPERIMENT

The Xe/Pt(997) adsorbate system was studied experimentally by thermal energy He scattering. This method allows the *in situ* determination of the growth mode in thin-film epitaxy.[12] Moreover, employing grazing incidence geometry, the method becomes very sensitive to the one-dimensional growth of rows attached to steps, as was recently demonstrated.[10,9] This sensitivity has been attributed to He reflectivity changes between complete and incomplete adsorbate rows at step edges.

The geometry of the perfect Pt(997) surface is shown in Fig. 1. The surface is obtained by cutting a bulk Pt crystal at an angle of 6.45° in the $\langle 11\bar{2} \rangle$ direction with respect to the

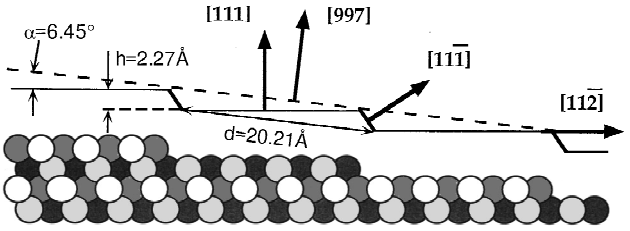

FIG. 1. Side view geometry of the bare vicinal (997) Pt surface; $\alpha = 6.45°$.

(111) close-packed surface.[13] The terraces are closed-packed (111) facets with a hexagonal lattice parameter of 2.77 Å, separated by monotomic $(11\bar{1})$ steps, 2.27 Å in height. The average terrace length is 20.21 Å with a distribution that is narrow due to step-step repulsive interaction.[14]

The measurements were performed with a high-resolution He scattering apparatus that allows rapid access to arbitrary scattering geometries between 60° and 180° total scattering angle. The dynamic range of detection is larger than four orders of magnitude. Figure 2 shows measurements of the specularly reflected He intensity as a function of coverage at different temperatures in grazing incidence geometry. Xe is adsorbed on the Pt(997) surface by backfilling the sample chamber with Xe at 3×10^{-8} mbar. The temperature dependence will be discussed in detail in Sec. IV. Here we focus on the bottom curve of Fig. 2 ($T=40$ K) and find that the intensity shows a rapid decrease of reflected intensity during build-up of coverages below 0.07 ML. During further adsorption the reflected intensity exhibits maxima at $\theta=0.14\pm0.02$ ML and $\theta=0.30\pm0.03$ ML. The appearance of maxima upon row completion is explained similarly to oscillations in layer-by-layer growth by the presence of a minimum of defects (i.e., kink sites in this case). The maxima are not due to mere interference effects because for different scattering geometries the peaks appear always at the same coverage. It is known that Xe on Pt(111) exhibits step decoration. Ordered structures are formed when adsorbate rows are completed. The peaks are found to broaden with increasing coverage. This is due to the variation of terrace width because larger terraces have a larger uptake of Xe atoms than smaller terraces have. In the following we will show that the coverage values can be explained well by the formation of complete rows.

The structure of Xe on Pt(997) at monolayer and submonolayer coverages has not yet been fully established. On a Pt(111) surface, Xe is known to form a commensurate $(\sqrt{3}\times\sqrt{3})R30°$ superstructure over a wide temperature and coverage range[11] with an average distance between nearest-neighbor atoms equal to 4.8 Å. If this structure was also the most stable on Pt(997) terraces, an average (997) terrace could thus accommodate seven or eight Xe rows parallel to the step edge. In order to determine the structure on the vicinal surface we measured He diffraction spectra. In Fig. 3(a) a diffraction scan in the $\langle 11\bar{2}\rangle$ direction from a Xe monolayer is shown for fixed incidence angle. The two intense diffraction peaks on the left-hand side are peaks due to specular scattering from the terraces. The peak splitting corresponds to the 20-Å periodicity of the surface. In this geometry diffraction peaks from the Pt row distance of 2.40

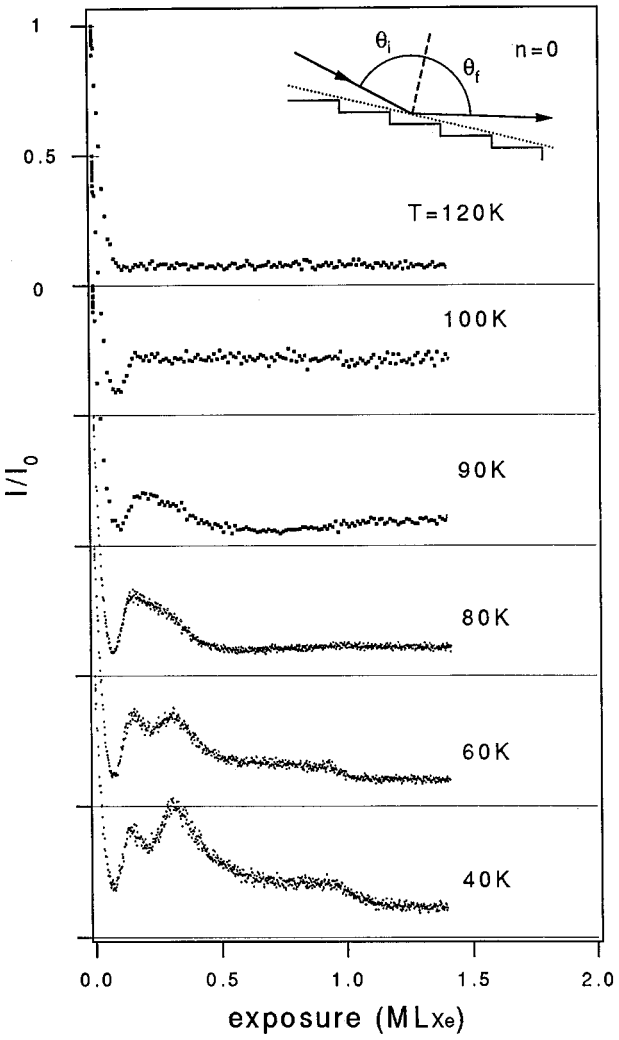

FIG. 2. Specular reflected He intensity at grazing angles ($\theta_i=\theta_f=76.2°$) as a function of Xe coverage on Pt(997). The measurements were made at the indicated surface temperatures. For the employed Xe background pressure of 3×10^{-8} mbar the exposure scale corresponds to a coverage scale for surface temperatures $T\leqslant 90$ K, $\lambda_{He}=1.03$ Å. The Xe monolayer coverage (ML_{Xe}) is defined as the coverage corresponding to a complete adlayer.

Å will not be visible as their total scattering angle χ exceeds 180°. The three peaks to the right of the specular peaks are due to diffraction from a Xe structure with a row distance that must be increased with respect to the substrate. The peak positions and the maximum of their intensity envelope contain the information on the Xe row distance. The peak spacing reflects again the surface periodicity. From an analysis of these peaks and peaks of diffraction scans in different geometries a Xe row distance of 3.87 Å is inferred. In a diffraction scan parallel to the $\langle 110\rangle$ direction, i.e., along the steps [Fig. 3(b)], a specular peak and a first-order diffraction peak are observed. The distance of 4.1 Å derived from these measurements corresponds to the nearest-neighbor distance in the Xe rows. The results of the diffraction measurements are attributed to a quasihexagonal structure with an average distance between nearest-neighbor Xe atoms equal to 4.3 Å. In this geometry, five close-packed Xe rows parallel to the steps cover a terrace. The structure is close to the one observed[6] by low-energy electron diffraction (LEED) for Xe/

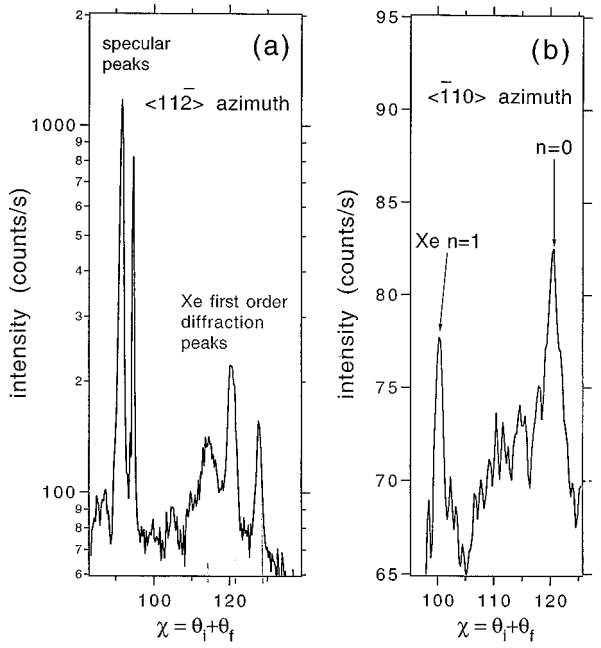

FIG. 3. Helium diffraction patterns for Xe monolayer coverage on Pt(997) at 45 K surface temperature, $\lambda_{He} = 0.93$ Å. (a) Scan for incidence angle $\theta_i = 59.3°$ and scattering plane perpendicular to the steps. From the evaluation of the three first-order diffraction peaks and their envelope a periodicity and thus a row-to-row distance of 3.87 Å is obtained. (b) Scan for incidence angle $\theta_i = 60.25°$ and scattering plane parallel to the steps. From the positions of the specular ($n = 0$) and first-order ($n = 1$) peaks the Xe-Xe distance parallel to the step of 4.1 Å is calculated.

Pt(332) a surface similar to Pt(997), but with a shorter terrace length. However, the He diffraction peaks become weaker for lower coverages and they cannot be observed below about 0.4 ML. A recent LEED study of Xe/Pt(997) (Ref. 15) found a Xe-Xe distance of 5.5 Å parallel to the steps for a coverage corresponding to a one-dimensional row of Xe atoms; this means that the Xe-Xe distance parallel to the steps should reduce from 5.5 Å for a single row to 4.1 Å for a complete monolayer.

The fact that the He reflectivity peaks appear at the coverages $\theta = 0.14$ and $\theta = 0.30$ and not at $\theta = 0.20$ and $\theta = 0.40$, respectively, as expected for a five closed-packed adsorbate rows parallel to the step, can have two reasons. First, the sticking probability may decrease with increasing coverage. This assumption, however, cannot explain the large discrepancy because the maxima of the layer-by-layer oscillations observed in nongrazing incidence appear at equal dosage intervals,[13] allowing changes in sticking coefficient of only a few percent. Second, a structural change may occur between the row and layer coverage. In fact, a conclusive explanation of the intensity maxima can be given on the basis of the structural change discussed above. In the first row the atom density for Xe is 1.81 atoms per nanometer step length, while at monolayer coverage the atom density increases to 2.58 atoms per nanometer in each row corresponding to a total of 12.90 atoms per nanometer for five rows. The coverage of the first row with respect to a complete monolayer is thus $\theta = 1.81/12.90 = 0.140$, in excellent agreement with the experimental result $\theta = 0.14$. Based on this model the position of the peak ascribed to the second row indicates that the density in the second row is equal to the one of the first row. Taking into account the observation that the diffraction peaks of the monolayer appear at about 0.4 ML coverage, the structural change may start after the completion of the second row.

Discrete-row growth at vicinal surfaces is expected to be a general phenomenon due to the increased binding energy of the adsorbate at step sites with respect to terrace sites. This is related to the increased coordination, which is particularly high at the bottom of the step, where in the case of Pt(997) the adsorbate has a minimum of five substrate atom neighbors instead of three on the terrace. It was recently argued, however, that Xe might prefer adsorption at low coordination sites and a scanning tunnel microscope (STM) study[16] suggests that already at low coverages Xe atom chains form at the top of isolated steps on Pt(111).

Our study strongly suggests that in the case of Xe/Pt(997), the rows observed by He scattering adsorb at the lower step edge. First, the decrease of intensity due to complete row adsorption is small at grazing incidence, indicating that the terrace that contributes also to the macroscopic specular reflection is not completely blocked. In certain geometries the first row peak is even more intense than the reflection from the clean surface.

Second, if the first row would be adsorbed on top of the step the row would cast a shadow that will not allow the observation of the repulsive part of the Xe-He potential of the second row at the bottom of the step. It is the strong corrugation of the repulsive potential and not a much weaker corrugation of the attractive part of the potential that determines the detectability of ordering in the rows.

Third, the analysis of diffraction intensities allows one to obtain information on the position of adsorption. The clean Pt(997) surface exhibits a diffraction pattern that is described by a lattice function times an envelope function.[17] The lattice function is determined by the surface periodicity leading to Dirac peaks of different diffraction orders. With increasing distance from the Bragg conditions of the three-dimensional Pt crystal lattice these peaks broaden due to the finite terrace width distribution. The integral intensity of different diffraction peaks is determined by the envelope function, which is in the simplest case approximated by the Fourier transform of a single plain terrace. Figure 4 shows the diffraction intensities for a clean surface and for a surface after adsorption of one and two rows. It is evident from these measurements that the envelopes for the completed rows are similar and that in comparison to the clean surface both are shifted towards larger scattering angles. In this nongrazing incidence geometry the second row becomes visible even if the first row would be adsorbed on top. The small difference between the envelopes for one and two Xe rows thus suggests that the second row adsorbs in a similar geometry to the first row. The shift of these envelopes with respect to the clean surface reflects a tilting of the effective repulsive potential towards the terrace plane. As shown in the insets in Fig. 4, this behavior also supports adsorption at the bottom of the step. For adsorption on top of the step the repulsive part of the Xe-He potential will increase backscattering towards lower exit angles, while in addition the He beam refraction leads to increased terrace bending, which still increases the shift. In

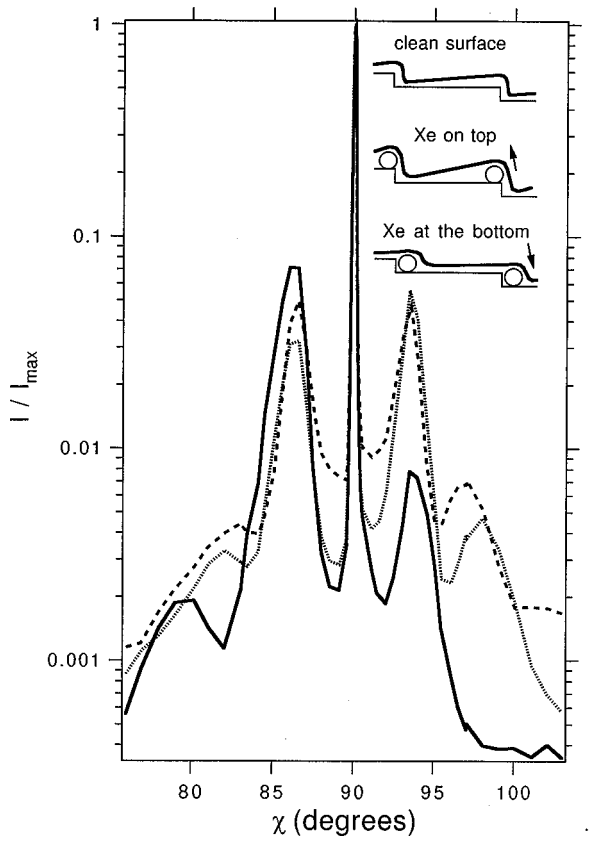

FIG. 4. Diffraction peaks of orders $n=-5$ (left) to $n=-1$ (right) for the clean Pt(997) surface (solid line) and for a surface on which one row (dashed line) and two rows (dotted line) of Xe were adsorbed at 45 K. Row completion was determined from the intensity maxima obtained in measurements such as that in Fig. 2. For an incident angle of $\theta_i=51.5°$ the total scattering angle $\chi=\theta_i+\theta_f$ was varied. With $\lambda_{He}=1.07$ Å the center peak at diffraction order $n=-3$ is sharp. Inset: shift of the effective terrace plane seen by the beam for the three indicated cases.

contrast, the adsorption at the bottom of the step may reduce the terrace bending and can explain an increased scattering towards larger exit angles.

Fourth, the STM study indicating decoration on top of isolated steps[18] demonstrates that the Xe atoms form rather discontinuous nuclei. Specifically, the STM image taken after Xe adsorption at higher temperature (30 K), which corresponds rather to our adsorption conditions (>40 K), indicates the formation of quite incomplete ''pearl chains.'' The observation of He intensity maxima, however, requires the growth of dense and continuous rows.

In Secs. III–V a detailed theoretical analysis of the submonolayer growth of Xe/Pt(997) is presented. In Sec. VI the discussion of experimental results will be resumed in comparison with the results obtained for the model.

III. INTERACTION POTENTIALS

A. Adsorbate-substrate interactions

As far as the interaction of rare gases with metal surfaces is concerned, difficulties are usually encountered in finding simple additive potentials that lead to results consistent with experimental data. For the Xe-Pt(111) system, many gas-surface potentials[19–26] have been used to test the accuracy of calculated quantities when compared to the available data including thermodynamic measurements, equilibrium and dynamical properties of adsorption, thermal desorption, trapping probabilities, and scattering measurements. Black and Janzen[23] used a number of different Pt/Xe corrugations without finding a Xe-Pt pair potential that simultaneously fits the experimental corrugations and the binding vibration frequency of xenon. Tully[19] studied also the accuracy of various pairwise potential forms (Lennard-Jones or Morse expressions) to describe the trapping dynamics of Xe on the Pt(111) surface. The flexibility of the pairwise potential forms was a required condition to recover the experimental corrugation and Xe-Pt(111) surface binding energy. Bethune, Barker, and Rettner[25] constructed a Xe-Pt potential from atom-atom sums that reproduces quite well the available experimental data, but they attributed a surprisingly small radius to the xenon atom.

Gottlieb and Bruch[20] proposed an effective interaction model for the system Xe/Pt(111) that reproduces the observed structural properties of the uniaxial incommensurate solid phase below 60 K. It consists of a Fourier amplitude representation for the lateral variation of the holding potential and a Lennard-Jones pair potential for the Xe-Xe interactions. The sign of the Fourier amplitude V_g discriminates the adsorption sites corresponding to atop and hollow Xe positions, but the barrier to lateral Xe motion was much smaller than the value inferred by experiments.[11] The distinction between atop and hollow adsorption sites has been investigated and local density functional theory applied to Xe adsorbed on small Pt clusters[27] showed that the equilibrium site would correspond to the atop position. Barker, Rettner and Bethune[26] then defined the Xe/Pt(111) interactions in terms of an empirical potential-energy function represented as a sum of nonspherical pairwise additive contributions with an additional contribution that describes the interaction with the delocalized conduction electrons in the metal. This potential was consistent with a wide range of dynamical and equilibrium experimental data and it led moreover to atop adsorption sites for Xe and to a Xe-surface distance about 3.3 Å, reasonably close to the values from *ab initio* calculations[27] or estimated from experiments.[22]

While the second species of potentials seem to be more accurate than the pair potentials for a comparison with most of the experimental data, they contain a nonlocal contribution schematized either by the Fourier amplitude describing the metal corrugation or by an exponential term function of the position of the local average surface that mimics the interaction with the delocalized metal conduction electrons. However, close to the step, such a contribution becomes invalid due to the singularity the defect creates at the surface. Therefore, either we can build a potential form containing a nonlocal parametrized contribution that accounts for the presence of the step or we go back to pairwise potentials that do not display such a drawback. A detailed experimental information on the Xe adsorption close to the step is clearly lacking and prevents a multiparameter fit of the nonlocal contribution. Here we thus consider the potential form discussed by Bethune *et al.*[25] because these authors calculate the adsorption energy of Xe in the vicinity of a close-packed step edge and test its adequacy to predict desorption rates.

The interaction Xe/Pt surface is derived from a Xe-Pt pair potential with parameters adjusted to fit the experimental values of the perpendicular vibrational frequency of Xe above the surface, the surface corrugation, and the adsorption well depth. These three latter quantities will play a dominant role in the calculations developed here. We will discuss the consequences of our potential choice on the interpretation of results in Sec. V.

The adsorbate-substrate potential is thus written as

$$V_{AS}=\sum_i \left(Ae^{-\alpha R_i}-\frac{C_6F(R_i)}{R_i^6}\right), \tag{1}$$

where R_i defines the distance between the adatom and the ith substrate atom. The first term represents the repulsion and the second contribution characterizes a damped dispersion interaction. The damping function $F(R)$ has the form used by Aziz and Slamann[28] for the Xe-Xe potential:

$$F(R)=\begin{cases} 1 & \text{for} \quad R\geqslant R_C \\ e^{-(R_C/R-1)^2} & \text{for} \quad R<R_C\,. \end{cases} \tag{2}$$

For the parameters occurring in Eqs. (1) and (2), Bethune *et al.*[25] used $A=55.64$ eV, $C_6=45.98$ eV Å^6, $\alpha=3.5$ Å^{-1}, and the cutoff distance $R_C=5.36$ Å. These values give a potential depth, a corrugation, and a perpendicular frequency that are fairly consistent with the experimental results of Kern *et al.*[11]

B. Adsorbate-adsorbate interactions

The interaction potential within the adsorbate is represented by a sum of pairwise atom-atom Lennard-Jones potentials

$$V_{AA}=4\varepsilon\sum_{k=6,12}\sum_{i,j}\frac{(-1)^{k/2}\sigma^k}{R_{ij}^k}, \tag{3}$$

where R_{ij} characterizes the instantaneous distance between the ith and jth adatoms. The values of the parameters ε and σ are equal to 24.9 meV and 3.885 Å, respectively.[29] Note that other contributions should be added to Eq. (3) in order to account for nonadditive three-body contributions, substrate-mediated interactions, and induction phenomena.[20] These contributions could provide corrections to the interaction potential; indeed, it was shown[30,31] that slight differences between the calculated and experimental lateral energies can arise from consideration of these additional interactions. However, the single potential given by Eq. (3) reproduces well the dynamical properties of the Xe adlayer adsorbed on other metal such as Cu (Ref. 32), and we thus disregard the influence of these small contributions for which accuracy remains questionable.

IV. EQUILIBRIUM CONFIGURATIONS FOR XENON

A. General

The first step in our investigation is the determination of the stable adsorption sites for the Xe atoms on the Pt(997) surface at 0 K. Let N be the number of such adatoms on a terrace. A gradient minimization procedure is used to calculate the equilibrium potential energy $V_{AS}+V_{AA}$ as a function of the $3N$ degrees of freedom of the adsorbate. When we consider a single Xe atom adsorbed on the vicinal surface, we get information on the holding potential V_{AS} in the stable adsorption site and the potential map $V_{AS}(X,Y)$ parallel to the surface. This information is then used to define the best strategy for studying the Xe growth, i.e., to determine whether xenon forms two-dimensional islands or three-dimensional aggregates on the Pt(997) terrace. While computation times are reasonably small for values of $N\leqslant 10$, it becomes necessary to limit the number of degrees of freedom for larger-N values, using symmetry arguments and information provided by the potential map $V_{AS}(X,Y)$.

B. Results

1. Single Xe adatom

Figure 5(a) represents the minimum potential-energy map experienced by a single Xe atom above the (997) Pt surface. The main characteristics determined here are close to those obtained by Bethune *et al.*[25] for the perfect surface. On a terrace, the most stable Xe site is the hollow site, i.e., when the rare-gas atom lies above the center of the regular triangle formed by three nearest-neighbor Pt atoms. The rare-gas atom lies 1.8 Å above the surface with a corresponding bonding energy of -255 meV. This surprisingly low value for the equilibrium height has been discussed already.[25] The average corrugation is 27 meV, a value that is consistent with the experimental one (30 meV) found by Kern *et al.*[11] The saddle point of the potential surface is the bridge position between adjacent Pt atoms.

Near a step, the Xe adsorption is modified since the potential valley perpendicular to the step direction exhibits a barrier on the upper terrace preventing the atom diffusion downstairs and on the lower terrace a trapping well deeper than the well obtained in the middle of a terrace. The minimum energy in the trapping site is equal to -352 meV. This value is 1.4 times larger than that for the adsorption on the terrace as a result of the increased coordination number of the adatom (roughly 5 for an atom close to the step instead of 3 on the terrace), which enhances the potential by a factor of about 5/3. In contrast, the Xe atom at the top of the step experiences a maximum potential energy equal to -130 meV. The influence of the step on the potential valley (trapping or chasing) extends over about two interatomic Pt-Pt distances, i.e., two rows of atoms parallel to the step. At the bottom ($Y\leqslant 0$), we clearly discriminate two different adsorption wells; one characterizes the first row of equilibrium sites parallel to the step [$Y=-(\sqrt{3}/2)a$] at -352 meV, while the sites in the second row ($Y=-\sqrt{3}a$) are less stable with an energy value of -260 meV. Beyond the second row, one finds still a small increment of the energy [Fig. 5(b)] superimposed on the oscillations that characterize the corrugation of the terrace. Analogously, at the top of the step ($Y\geqslant 0$) two different adsorption sites close to the step have higher energies than perfect terrace sites with the corresponding values -226 and -250 meV for the first and second rows, respectively. Beyond this distance, the energy increment becomes vanishingly small.

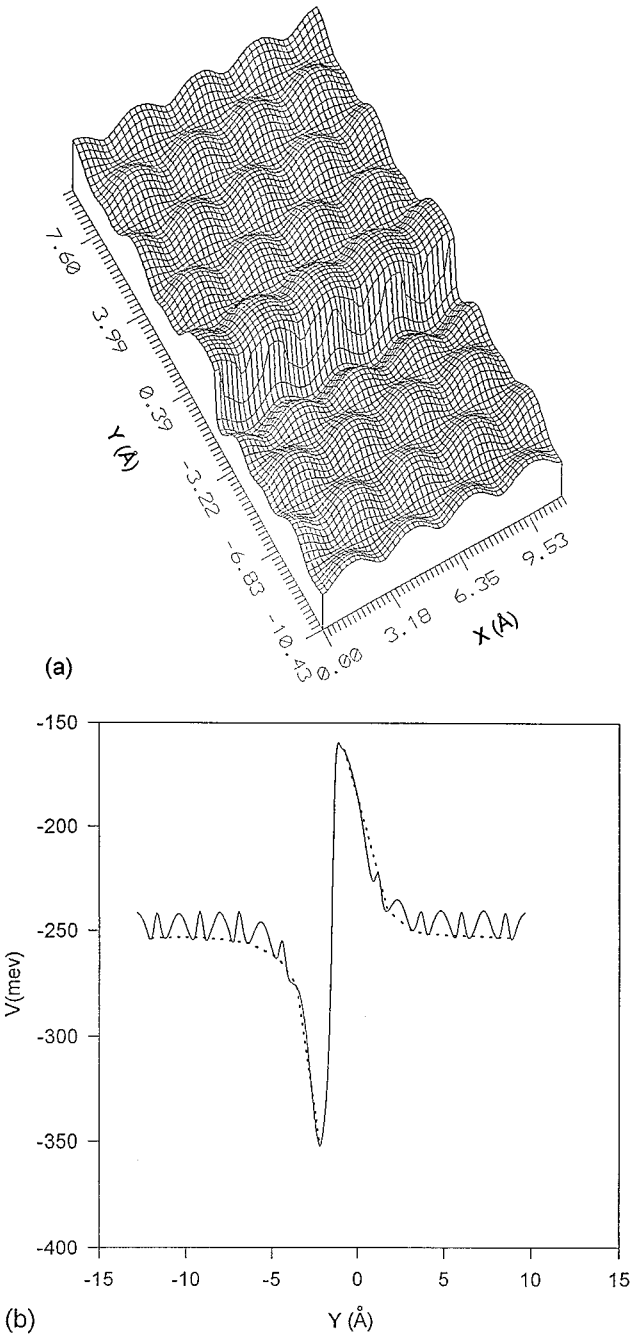

FIG. 5. (a) Equilibrium potential-energy surface $V_{AS}(X,Y)$ (in meV) experienced by a single Xe atom adsorbed on both sides of a step. (b) Diffusion valley for a Xe atom moving perpendicular to the step. The mean potential increment due to the influence of the step is drawn using dotted lines.

2. Xe growth on a terrace

The minimization calculations at 0 K for several adatoms show that the lateral potential remains in general weak when compared to the corrugation characterizing the holding potential. The Xe atoms tend to fill the trapping sites along the first line at the bottom of the step, as mentioned before. In this configuration, along the step, they are equally spaced by a distance $2a \simeq 5.54$ Å, as shown in Fig. 6(a). This structure is in full agreement with LEED observations.[15] Each adatom has a potential energy of -363 meV; the lateral contribution is equal to 11 meV and represents only 3% of the total potential.

When the first row is completely filled (Xe coated step) we continue to add Xe atoms and obtain two new features. First, because of the still deep potential well in the second line (-260 meV), the adatoms are trapped in this row with an energy equal to -286 meV. The lateral contribution increases since it represents 7% of the total energy. Second, a reconstruction of the first Xe row occurs due to the influence of the second line. Indeed, though the lateral interactions are weak, they force the first line atoms to move apart and to become spaced by a distance $3a$ instead of $2a$, as shown in Fig. 6(b). In other words, the stabilizing influence of the lateral interactions of the second-row atoms on the first-row structure compensates for the Xe-Xe interactions inside the first line. Then, if one adds more and more Xe atoms, the ''row-by-row'' growth process evolves monotonically. After the two previous lines are filled, the energy increment due to the step disappears and all the sites have the same depth. It is only the lateral contribution that can explain the row-by-row growth by enhancing the coordination number of adatoms. When the coverage rate is close to the terrace completion, the structure of this confined layer is the $(\sqrt{3}\times\sqrt{3})R30°$ phase [Fig. 6(c)] of the monolayer adsorbed on the Pt(111) surface without defect. The nearest-neighbor Xe-Xe distance is $a\sqrt{3}$ with the primitive translation vectors rotated by 30° with respect to the substrate vectors.

At this stage, let us call $\{(l,m)\}$ the set of available adsorption sites. Each (l,m) couple characterizes the mth site belonging to the lth line parallel to the step direction. A terrace is thus defined by the row number $l=1,\ldots,8$ and the intrarow site number $m=1,\ldots,\infty$ since there are eight rows parallel to the step, each containing an infinite number of sites. The holding energy of each site (l,m) is labeled V_{lm}, which reduces to V_l since we have shown that each site in a given line has the same energy, namely, $V_1=-352$, $V_2=-260$, $V_{i=3,6}=-255$, $V_7=-250$, and $V_8=-226$ meV. The lateral energy γ between two nearest-neighbor Xe atoms is significantly smaller and equal to -22 meV.

For a coverage less than the completion, the adatoms do not adsorb at the top of the step because the Xe-Xe interactions cannot compensate for the holding energy difference in this configuration when compared to the adsorption on the lower terrace. Moreover, the nearest-neighbor distance between two Xe atoms belonging respectively to the upper and lower terraces is larger than the Xe-Xe distance $(a\sqrt{3})$ on a terrace. As a consequence, we can neglect the interactions between Xe atoms belonging to adjacent steps and assume that the adsorption phenomenon on a terrace is independent of what happens on another terrace.

To end this section we will make two main comments on these results. First, the occurrence of the commensurate $(\sqrt{3}\times\sqrt{3})R30°$ Xe geometry is the consequence of the form of the selected potential for V_{MS}. Indeed, the rather large corrugation it gives is consistent with the existence of commensurate rather than incommensurate structures. Decreasing arbitrarily the surface corrugation would favor the incommensurate structure. Second, the large row number on the Pt(997) terrace (eight with the commensurate structure) is

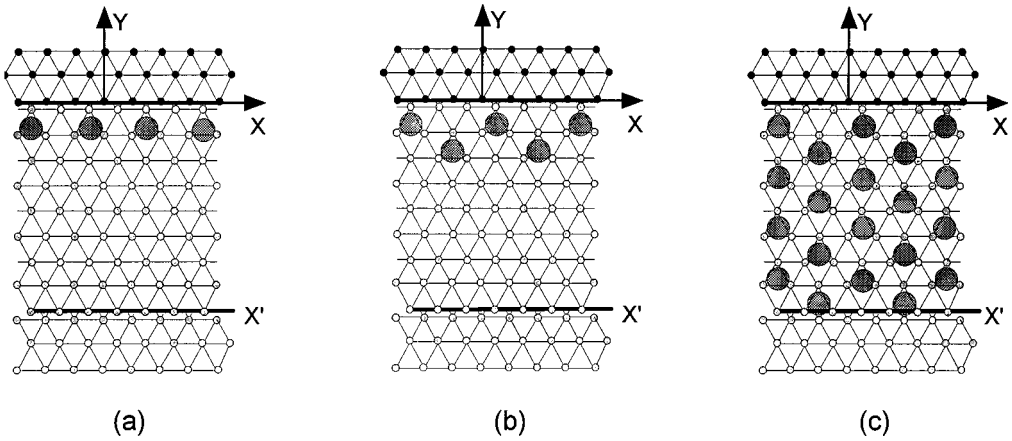

FIG. 6. Equilibrium geometry of Xe atoms adsorbed at various coverages on a confined terrace of Pt(997). The upper terrace is along the X axis and the lower terrace is along X'. The hatched circles schematize the Xe atoms: (a) ordering in the first row, (b) two-rows geometry, and (c) layer completion on the confined terrace with the $(\sqrt{3}\times\sqrt{3})R30°$ geometry.

the result of the small Xe-step distance (2.4 Å) displayed by this potential, a drawback already discussed for the value of the height of Xe above the surface. Increasing reasonably the Xe step distance would decrease the row number to 7. Therefore, to be consistent with our potential choice, we will study the Xe growth at finite temperature within the scheme of the commensurate $\sqrt{3}\times\sqrt{3}$ geometry. Nevertheless, we will discuss how the model is quantatively (but not fundamentally) modified by changing the corrugation and the Xe-step distance.

V. STRUCTURE GROWTH AT FINITE TEMPERATURE

Using information on the equilibrium arrangement of the Xe adatoms, we consider now the influence of temperature on the adsorption process. More precisely, we study the coverage change with the chemical potential $\mu(p,T)$ of the xenon gas phase; p and T are the gas pressure and temperature, respectively. We use a grand-canonical distribution to describe the thermodynamic properties of the Xe system that accounts for the exchange of Xe atoms between the gas state and the adsorbate state. The metal is assumed to be rigid and undeformed.

A. Ideal lattice-gas model

As the lateral potential remains weak when compared to the holding contribution, we first assume an ideal lattice-gas model to describe the adsorbate/substrate system. Within this approach, we associate with each adsorption site a probability 0 or 1 to be occupied by a xenon atom. We then use the results of Sec. IV B and define an exclusion surface S_e for each site equal to $S_e=3\pi a^2$ since the nearest-neighbor distance between sites is $a\sqrt{3}$. Note that we do not take into account the singularity of the first-row growth. Indeed, we have seen in Sec. IV that at 0 K the atoms in the first row are spaced by a distance $2a$ instead of the $3a$ in the other rows. As a consequence, the density in the first row would be different from the others. But, at finite temperature, we are more concerned by a kinetic problem than a static one and it thus appears more realistic to assume that all the atoms are equally averaged spaced.

The grand partition function $\Xi(\mu,T)$ is written as a simple product of the partition functions associated to any site as

$$\Xi=\prod_{l,m}\left[1+e^{-\beta(V_{l,m}-\mu)}\right]. \tag{4}$$

The grand potential $J=-\beta^{-1}\ln\Xi$ allows us to express the mean number $\overline{N_{l,m}}$ of Xe atoms that occupy the (l,m)th site as a fermionlike occupation function

$$\overline{N_{l,m}}=\frac{1}{\left[1+e^{\beta(V_{l,m}-\mu)}\right]}. \tag{5}$$

The mean coverage θ of a terrace, defined as the ratio of $\overline{N_{l,m}}$ and the available adsorption site number $N_{S,}$ is thus given as

$$\theta(\mu,T)=\frac{1}{L}\sum_{l=1}^{L}\theta_l(\mu,T)=\frac{1}{L}\sum_{l=1}^{L}\frac{1}{1+e^{\beta(V_l-\mu)}}, \tag{6}$$

where L is the number of Xe rows on the terrace and $V_{l,m}=V_l$ for all m (Sec. IV). θ appears as a sum of the coverages $\theta_l(\mu,T)$ per row.

The behavior of the adsorption isotherms $\theta_T(\mu)$ for various temperatures leads to information on the Xe growth process on a confined terrace. The shape of $\theta_T(\mu)$ is formed by successive steps that are more or less apparent, depending on the line number l and on temperature. Each step corresponds to the growth of a row, while each terrace represents the stability range of a completed row.

Let us then define the isothermal compressibility K_T of the adsorbate as

$$K_T=-\frac{1}{A}\left(\frac{\partial A}{\partial\phi}\right)_T, \tag{7}$$

where ϕ is the adsorbate spreading pressure and $A=N_S S_e\theta$ characterizes the adsorbate surface. After straighforward manipulations, we can write

$$K_T = N_S S_e \chi(\mu,T) = N_S S_e \left(\frac{\partial\theta}{\partial\mu}\right)_T \tag{8}$$

and find the expression for $\chi(\mu,T)$ using Eq. (6) as

$$\chi(\mu,T) = \frac{\beta}{4L}\sum_l \frac{1}{\cosh^2\left(\beta\dfrac{V_l-\mu}{2}\right)}. \tag{9}$$

The function $\chi(\mu)$ appears as a set of Dirac peaks located at the values $\mu = V_l$ ($l = 1,2,\ldots,8$) for $T = 0$ K. These peaks broaden at finite temperature with a full width at half height equal to $\Delta = 4 \arg\cosh(\sqrt{2}) k_B T \simeq 3.52 k_B T$. The condition for peak resolution indicating row-by-row growth leads us to define a criterion for temperature that can be written as

$$T_{r_l} = \frac{|V_{l+1} - V_l|}{3.52 k_B}, \tag{10}$$

where T_{r_l} characterizes the maximum temperature required to observe the occurrence of the lth xenon row. In other words, for $T \leqslant T_{r_l}$, we can distinguish the ordering of the lth row with respect to the $(l+1)$th one. Beyond this value, $T > T_{r_l}$ every adsorption site on the lth or $(l+1)$th row is equivalent for Xe atoms.

B. Mean-field Hamiltonian Ising model

To improve the previous model that is valid within the assumption of vanishing lateral interactions between Xe atoms, we use a conventional two-dimensional Ising model with a Hamiltonian H defined as

$$H = \sum_{l,m} V_l \sigma_{l,m} + \gamma \sum_{l,m,l',m'} \sigma_{l,m}\sigma_{l',m'}, \tag{11}$$

where $\sigma_{l,m}$ characterizes the atom number occupying the (l,m)th adsorption site and γ is the lateral interaction between two Xe atoms adsorbed in nearest-neighbor sites. Let us then define an effective mean potential experienced by a Xe atom trapped in the (l,m)th site as

$$\overline{V^*_{l,m}} = V_l + \gamma \sum_{l',m'} \overline{\sigma}_{l',m'}. \tag{12}$$

The sum is restricted to the coordination number associated with a given site (l,m) and $\overline{\sigma}_{l',m'}$ describes the mean occupation of the (l',m') site. The grand partition function Ξ [Eq. (4)] is changed by substituting $V_{l,m}$ by $\overline{V^*_{l,m}}$ and we thus obtain in a straightforward way the mean coverage $\theta_l(\mu,T)$ for the lth row as

$$\theta_l(\mu,T) = \frac{1}{1 + e^{\beta[V_l - \mu + \gamma(\theta_{l-2} + 2\theta_{l-1} + 2\theta_{l+1} + \theta_{l+2})]}}. \tag{13}$$

In Eq. (13) we have considered that each atom experiences the lateral interactions with its six nearest-neighbor atoms located inside the $l \pm 1$ and $l \pm 2$ rows. This equation is self-consistent and cannot be solved analytically, in contrast to Eq. (6). Nevertheless, to proceed further, we can replace, in a first approximation, the expressions for $\theta_{l'}(l' = l \pm 1, l \pm 2)$ by those determined in the lattice-gas approach [Eq. (6)]. We thus obtain a closed expression for $\theta_l(\mu,T)$ that depends on the set of parameters $(V_l, V_{l'}, \gamma)$ characterizing the holding and lateral interactions. This expression is used in the numerical application.

C. Numerical results

In Fig. 7 we show the behavior of the coverage as a function of the chemical potential μ for three characteristic temperatures [Eq. (13)]. At low temperature ($T = 10$ K), Fig. 7(a) exhibits the striking discrete stepwise behavior of the coverage, already mentioned in the lattice-gas model. There are six significant θ values defining slope breakings in the curve at $l/8$ with $l = 1,2,3,4,7$, and 8. These particular values of the coverage correspond to the completion of a given row. This means that we can distinguish independently the growth of these rows. By contrast, for the intermediate rows of the terrace ($l = 5$, 6, and 7), the adsorption sites are equally probable and the site occupation is random, irrespective of the row number. At intermediate temperature ($T = 30$ K), the number of distinct slope breaks for the curve $\theta(\mu)$ decreases and only the rows with $l = 1,2,3,7$, and 8 can be distinguished [Fig. 7(b)]. At higher temperature ($T = 60$ K), the discrete growth can occur only for the first two rows close to the step where the potential increment is significantly large. For the other sites, the coverage increases quasicontinuously with μ [Fig. 7(c)] indicating randomization. At $T = 100$ K, only the first-row growth process can be observed in the curve (not drawn).

To interpret the occurrence of the two types of growth processes on the confined terrace (the discrete row-by-row growth and the random growth) one may note that the resulting behavior of the coverage as a function of the chemical potential appears to be similar in the two approaches (Secs. V A and V B). Thus, even though the lateral interactions play a significant role in these processes, they do not alter the main features. The competition between the potential increment due to the upper and lower steps as experienced by the Xe adatoms confined on the terrace and the thermal energy β^{-1} is responsible for this phenomenon. Indeed, when the potential increment $|V_{l+1} - V_l|$ is significantly larger than β^{-1}, the energy that a Xe atom gains (or loses) by adsorbing on sites of a given row tends to favor the inter-row competition and thus the discrete-row growth. In contrast, when $|V_{l+1} - V_l|$ is vanishingly small, the adsorption sites become equiprobable and the growth is random.

There are two main differences between the ideal lattice-gas model and the mean-field approach. First, as seen in Fig. 7, the chemical potential μ_l connected to the occurrence of the lth row is not equal to V_l, as it is in the lattice-gas approach. Second, the temperatures T_r listed in Table I for which the discrete-row growth can be distinguished are significantly different for the two models. These two features are closely related, although it is not straightforward to understand their origin since only a numerical procedure can

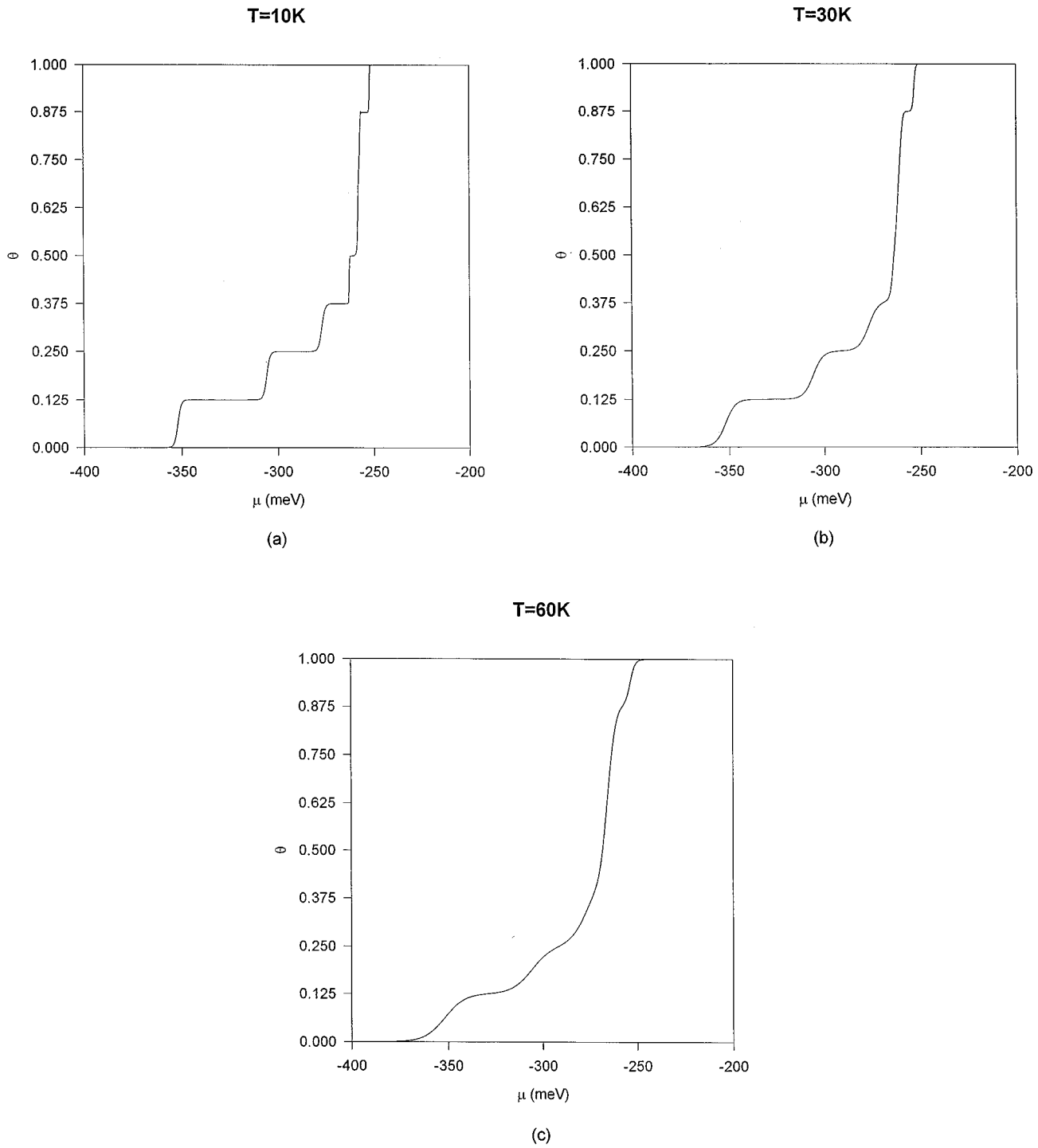

FIG. 7. Coverage θ vs chemical potential μ for three characteristic temperatures $T=10$ (a), 30 (b), and 60 (c) K. Note the stepwise behavior of the growth and the progressive disappearance of this feature when T increases.

allow us to solve this problem. From Eq. (13), μ_l satisfies the equation

$$\frac{\mu_l - V_l}{2\gamma} = \frac{1}{2}\sum_{i=l-2}^{l+2}\frac{1}{1+e^{\beta(V_i-\mu_l)}} + \frac{1}{2}\sum_{i=l-1}^{l+1}\frac{1}{1+e^{\beta(V_i-\mu_l)}} - \frac{1}{1+e^{\beta(V_l-\mu_l)}} \tag{14}$$

and it thus depends on the relative magnitudes of the potentials $\gamma, \Delta V_1 = V_l - V_{l-1}$, and $\Delta V_2 = V_l - V_{l-2}$ and of the thermal energy β^{-1}. For instance, we present in Fig. 8 the situations occurring for the third and fifth rows. The straight line with negative slope $1/2\gamma$ ($\gamma \leqslant 0$ means attractive lateral interactions between Xe atoms) intersects the curve defined by the right-hand side of Eq. (14) and gives the root μ_l of Eq. (14). For the third row [Fig. 8(a)], we see that the chemical potential is almost independent of T within the range of

TABLE I. Temperatures T_r (K) indicating a row-by-row xenon growth.

Row	Lattice-gas model	Ising model	
	$\sqrt{3}\times\sqrt{3}$	$\sqrt{3}\times\sqrt{3}$	Incommensurate
1	296	130	155
2	23	90	90
3	0	45	5
4	0	20	5
5	0	2	
6	16	5	
7	79	85	
8			

temperature considered here. Indeed, the straight line intersects a plateau of the curve leading to the situation for which $\Delta V_1 \leqslant |\gamma| \leqslant \Delta V_2$; μ_3 is then approximately equal to $V_3+\gamma$. By contrast, for the fifth row [Fig. 7(b)], one has $|\gamma| \geqslant \Delta V_1$ and $|\gamma| \geqslant \Delta V_2$ and μ_l depends drastically on the temperature since the straight line intersects a nearly vertical line connecting two plateau. No analytical solution can be determined in this case. For the other rows, the analysis is still more intricate since it depends on the length of the plateau, but the solutions μ_l are always lower than the V_l values determined in the ideal lattice-gas model. Note that even if the lateral interaction characterized by $|\gamma|$ is small when compared to the holding potential, it propagates the step effect to all the rows. At zero temperature, we therefore see the growth of all the rows with the mean-field Hamiltonian Ising approach, while it is not the case in the ideal lattice-gas model for which rows $l=3-6$ have the same holding potential.

As a consequence of the negative shift of the μ_l roots of Eq. (14) with respect to V_l, the temperatures T_r obtained in the Ising approach are significantly different from those obtained in the lattice-gas model (Table I). More specifically, we see that the third, fourth, and fifth rows can be distinguished below temperatures equal to 45, 20, and 2 K, respectively, whereas they are not distinguished in the ideal lattice-gas approach. The temperatures T_r can be greater or smaller than those obtained by the lattice gas depending on the relative values of γ, T, ΔV_1, and ΔV_2. The first row can be distinguished up to 130 K, while the second row occurs for T less than 90 K. The sixth row disappears for a temperature higher than 5 K. The last row ($l=8$) corresponds to the completion of the terrace, which is obtained when the seventh row is filled; this is observed for T less than 85 K. The mean-field model discussed so far describes the probability of finding an atom in each row for a given total coverage. However, the lateral interaction in the adsorbate can give rise to different characteristic structures of the adsorbate step edge, which we will briefly sketch. Preliminary Monte Carlo simulations with potentials similar to one given in Sec. III demonstrate that at coverages corresponding to less than four complete rows the adsorbate step edge rowing becomes random with increasing temperature. At higher coverages, the adsorbate begins to exhibit a zigzag step edge with straight sections parallel to close-packed directions in the $(\sqrt{3}\times\sqrt{3})R30°$ structure. The formation of close-packed adsorbate step edges may thus drive thermally induced faceting of the growing front.

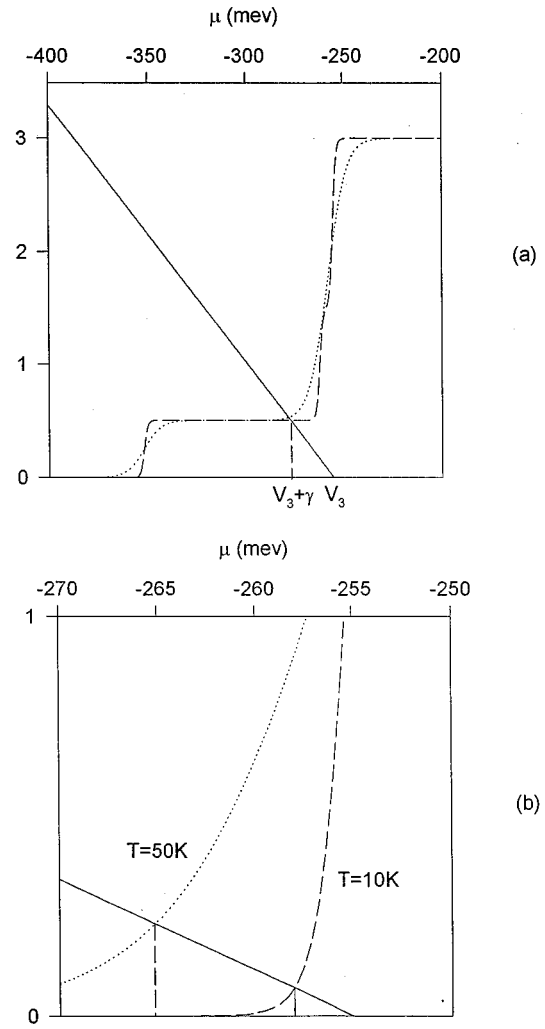

FIG. 8. Graphical resolution of Eq. (14) showing the dependence of the critical chemical potential μ_l vs temperature for (a) a well-resolved plateau corresponding to the third row completion and (b) for a very limited plateau corresponding to the fifth row (see the text).

VI. DISCUSSION

In this section we compare the measurements and the results for the potential model presented in the previous sections. As already discussed in Sec. II the coverage-dependent reflected He intensity exhibits at 40 K surface temperature two maxima that correspond to the first and the second completed rows (Fig. 2). For the potential used in Secs. III–V, preferential Xe adsorption is obtained at the lower step edge, in agreement with the experimental result discussed in Sec. II. The model predicts a Xe-Xe distance in the first row of 5.5 Å. This value was found experimentally in a LEED study by Trischberger and co-workers.[15] The quasihexagonal incommensurate structure with five rows in a monolayer could

not be reproduced by the calculation. The difference between calculation and experimental results indicates that the Xe-Xe interaction (leading to an incommensurate structure) and the step-Xe interaction (which leads to the formation of close-packed Xe rows parallel to the steps) are more important than the corrugation of the Pt-Xe potential on the terrace.

The temperature dependence of the growth process was studied experimentally for a series of surface temperatures above 40 K shown in Fig. 2 (see also Ref. 9). From these measurements, lower limits of the critical temperatures for the discrete row growth can be obtained. At a gas pressure of 3×10^{-8} mbar, Xe exhibits multilayer growth below a substrate temperature of 57 K. Below 91 K equilibrium with the gas phase occurs only after the completion of a full monolayer.[13] Here ordered rows are formed only in a transitory state during continuing adsorption. The first-row peak in Fig. 2 is visible up to 90 K. At 100 K the intensity reaches this peak and then stays constant, indicating that the equilibrium between the complete first row and the gas phase is reached. The second peak becomes smeared out above 80 K. Although up to 100 K adsorption continues after the formation of the first row, the second row does not appear as a distinct peak and thus is not completed before the third row begins to grow. Discrete-second-row formation is thus observed up to 80 K.

The experimental estimates of these characteristic temperatures T_r and the results for the Ising model (Table I) agree nicely. As a general trend, the experimental values are lower, indicating that only lower limits for discrete-row growth are obtained. One has to bear in mind that in the experiment the three-dimensional Xe pressure is constant and coverage increases as a function of time. The experiments were not performed in equilibrium between the gas phase and adsorbate, which would correspond to constant chemical potential conditions. Specifically in the case of the first row where the difference between the experimental value (100 K) and model (130 K) is large, an ordered row may still form at higher temperature if an increased ambient pressure provides a sufficiently high coverage. A second aspect is important for the comparison between the experiment and model: In an experiment discrete rows may not form even though they correspond to equilibrium states because the kinetics of the growth process will play a role, e.g., at low temperature or high deposition rate. Taking into account the difference in the monolayer structure between calculation and experiment, the agreement in the thermodynamic data is fairly good. The structural details do not appear to be essential in determining the thermodynamics of growth in this system.

Our calculations for the Xe/Pt(997) system can also be compared to numerical calculations performed by Merikoski *et al.*[8] In their paper, they consider a linear dependence of the potential-energy increment due to the step as a function of the distance with respect to the step. They also assume that the lateral interaction (γ parameter) is larger than the holding potential. At low temperature, they obtain a discrete growth for all the rows of the terrace because the step potential value is different for each row. But, due to the linear dependence of the holding potential, they determine a single characteristic temperature T_r. Our model differs fundamentally from this linear model since (i) the lateral interactions are weak when compared to the holding energies (this is specific to the xenon adsorption on Pt) and (ii) the energy increment is exponential rather than linear, as shown in Fig. 5(b). The first condition leads us to take advantage of the mean-field approach, which should not be valid for large-γ values, i.e., for other adsorbates and/or substrates. The second situation clearly appears to be much more physical since nonlinear behavior is responsible for the occurrence of several critical temperatures, as verified from the comparison with experiments.

Improvements of the calculations could be done on the accuracy of the values of the T_r temperatures by using a transfer-matrix method[8] to solve the self-consistent equation [Eq. (13)]. The mean coverage would be determined by overcoming the approximations tied to the mean-field Hamiltonian in the Ising model. But the main point of discussion is the influence of the potential choice on the model developed here to interpret the row-by-row growth of Xe/Pt(997). The Xe-Pt potential can account for the observed geometry of the first row with a mean Xe-Xe distance along the step equal to 5.54 Å. If the corrugation was arbitrarily decreased down to zero on the terrace, we would obtain a considerably smaller ($\simeq$4.4 Å) mean distance in the first row imposed by the lateral interactions in the incommensurate phase. The present potential with the large corrugation leads to the stable $(\sqrt{3}\times\sqrt{3})$ commensurate structure that is experimentally observed on larger terraces and at temperature higher than 60 K. Moreover, STM measurements[33] on Xe/Pt(111) have evidenced a 30° rotated structure attached to the steps. This structure, most probably the $(\sqrt{3}\times\sqrt{3})R30°$ structure, is observed in regions where the step is rough or the step direction deviates sufficiently from the $(11\bar{1})$ direction. The mean Xe-Xe distance in this structure is slightly larger (4.8 Å) than for the incommensurate phase inferred from He scattering experiments with an intrarow Xe distance of 4.1 Å and an interrow distance of 3.87 Å, leading to an average Xe-Xe distance equal to 4.3 Å. One such quasihexagonal structure for which the (997) terrace could accommodate five Xe rows is shown in Fig. 9(a). The potential increment, due to the step and counterstep, experienced by an adatom on a terrace without corrugation is presented in Fig. 9(b). The equilibrium distance between the first Xe row and the step is equal to 2.4 Å. At this distance, the step influence is maximum; then it decreases quickly to vanish around 8 Å, while the influence of the counterstep becomes significant above 14 Å. According to the model presented in Sec. V B, modified to account for the number of nearest-neighbor adatoms [see Fig. 9(a)], we calculate the corresponding temperatures T_r and obtain the values given in column 3 of Table I. Only the discrete growth of the first two rows could be observed within this scheme. Indeed, the second row is located at 6.3 Å from the step with a step potential less than 10 meV, instead of 90 meV for the first row [Fig. 9(b)]. For these two rows, the temperatures T_r are not very different from those obtained with the commensurate structure and are still in fair agreement with experiments.

Previously, we mentioned that the potential used here gives, furthermore, a Xe-Pt distance on the terrace that is small. This drawback is also present to a lesser extent for the

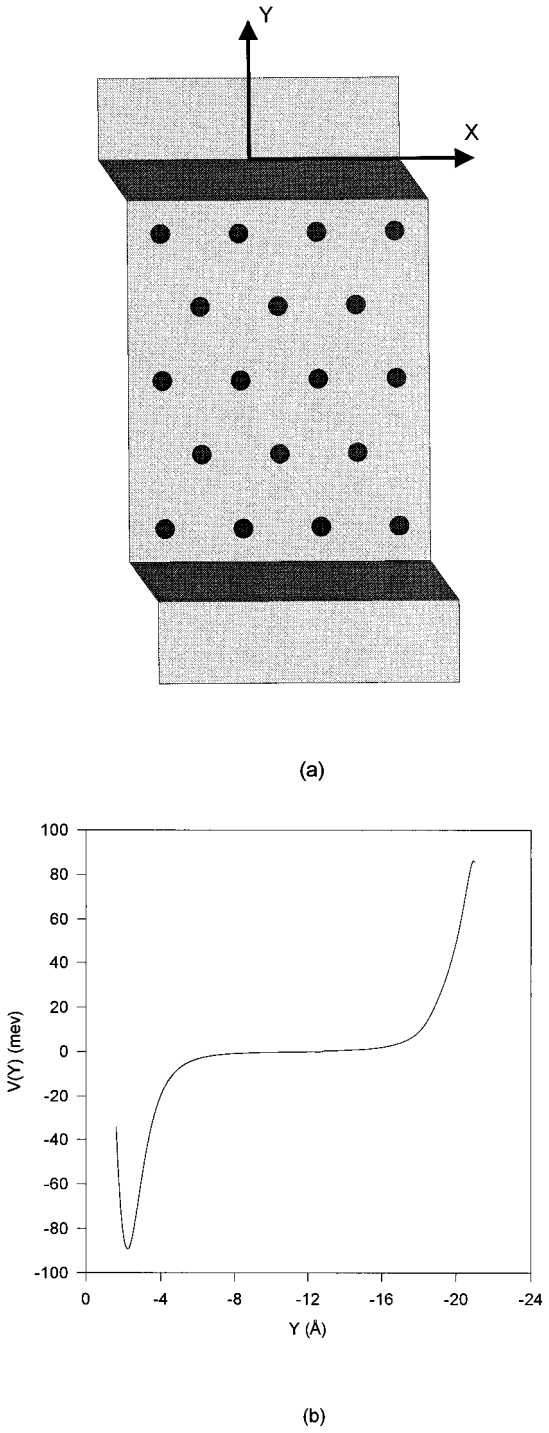

FIG. 9. (a) Quasihexagonal geometry inferred from experiments: five Xe rows with an average Xe-Xe distance equal to 4.3 Å. (b) Potential increment experienced by a Xe atom and due to the step and counterstep vs the distance with respect to the step.

Xe-step distance equal to 2.4 Å. The equilibrium site at the step, with the distance value of 2.4 Å, corresponds to a stable site for the $(\sqrt{3}\times\sqrt{3})$ commensurate phase and for the substrate without corrugation. If we expected larger distances from the step, the next hollow site would be at 4.0 Å; this value appears to be too large when compared to the inferred values from calculations and experiments, within the range 3.0–3.5 Å. Thus, changing the potential form would result in equilibrium sites at distances ranging between 3.2 Å from the step for atop positions and 4.0 Å for the next hollow positions, which would lead first to a geometry change of the confined layer and second to a change of the number of rows.

However, we must keep in mind that the major phenomenon that is considered from a theoretical point of view is the thermodynamic description of the Xe ordering during the growth on a confined terrace. We have seen that two main parameters determine the behavior of the row-by-row ordering: the value of the lateral pairwise interaction γ and the increment of the atom-surface potential ΔV_l as a function of the Xe distance with respect to the step. The first parameter γ is not very sensitive to the Xe-Xe distance within a reasonable range of values: γ takes the values 19, 25, and 22 meV when the Xe-Xe distance changes from 4.1 to 4.4 and 4.8 Å, respectively. The influence of the second parameter ΔV_l appears more difficult to evaluate since the form of the holding potential defines both the slope and the magnitude of the increment ΔV_l $(l=1,2,\ldots)$. What can be said is that the slope is mainly connected to the long-range part of the potential, which should not be very different for the various potential forms. If the potential well depth at the equilibrium site close to the step is calibrated with the same value, for Xe-step distances equal to 2.4 Å and 3.2 Å, for instance, the increment magnitude is also expected not to change in a dramatic way, being only a scale translation on the distance. As a consequence, the calculated row-by-row temperatures T_r should not be fundamentally modified. Note, however, that if the Xe-step distance increases, the number of rows on the confined terrace should decrease.

VII. SUMMARY

The discrete-row growth of Xe/Pt(997) that was observed by grazing incidence He scattering was modeled for realistic adsorbate-substrate and adsorbate-adsorbate interaction potentials. A discrepancy is found for the Xe monolayer structure that is obtained to be commensurate in the calculation, while He diffraction measurements indicate an incommensurate structure. The discrepancy is probably due to an overestimated value of the corrugation given by the selected potential. In theory and experiment the attachment of the rows takes place at the bottom of the steps and both agree to the Xe-Xe distance value in the first row adsorbed at the step. The temperatures of complete row formation are in good agreement with the experimental results, thus indicating that the potential corrugation is not the dominant parameter involved in the rowing process. In fact, it is shown that the major effect is the shape of the potential increment due to the step and counterstep. Extensions of these results to adsorption of small molecules on vicinal surfaces of metal oxides or dielectrics could be planned since it has been shown[34] that steps play a similar trapping role for the first stages of growth, with, nevertheless, an increasing influence of the lateral interactions due to electrostatic contributions.

*Electronic address: cgirardet@univ-fcomte.fr
†Permanent address: Fritz-Haber-Institut der Max-Planck-Gesellschaft, D-14195 Berlin, Germany.

[1] *Phase Transitions in Surface Films*, edited by J. G. Dash and J. Ruvalds (Plenum, New York, 1980); *Phase Transitions in Surface Films 2*, edited by H. Taub *et al.* (Plenum, New York, 1991); *Kinetics of Ordering and Growth at Surfaces*, edited by M. G. Lagally (Plenum, New York, 1990).
[2] M. Bienfait, Surf. Sci. **162**, 411 (1985).
[3] J. Lapujoulade, in *Interaction of Atoms and Molecules with Solid Surfaces*, edited by V. Bortolani, N. H. March, and M. P. Tosi (Plenum, New York, 1990), p. 381; K. Wandelt, Surf. Sci. **251/252**, 387 (1991).
[4] G. A. Bassett, Philos. Mag. **3**, 1042 (1958).
[5] H. Bethge, Surf. Sci. **3**, 33 (1964).
[6] B. Cathrine, D. Fargues, M. Alnot, and J. J. Ehrhardt, Surf. Sci. **259**, 162 (1991).
[7] R. Miranda, S. Daiser, K. Wandelt, and G. Ertl, Surf. Sci. **131**, 61 (1983).
[8] J. Merikoski, J. Timonen, and K. Kaski, Phys. Rev. B **50**, 7925 (1994).
[9] V. E. Marsico, M. Blanc, K. Kuhnke, and K. Kern, Phys. Rev. Lett. **78**, 94 (1997).
[10] M. Blanc, V. E. Marsico, K. Kuhnke, and K. Kern (unpublished).
[11] K. Kern, R. David, R. L. Palmer, and G. Comsa, Phys. Rev. Lett. **56**, 620 (1986); K. Kern, R. David, P. Zeppenfeld, and G. Comsa, Surf. Sci. **195**, 353 (1988) and references therein.
[12] B. Poelsema, A. F. Becker, G. Rosenfeld, R. Kunkel, N. Nagel, L. K. Verheij, and G. Comsa, Surf. Sci. **272**, 269 (1992).
[13] V. E. Marsico, Ph.D. thesis, Ecole Polytechnique Féderale de Lausanne, 1995.
[14] E. Hahn, H. Schief, V. E. Marsico, A. Fricke, and K. Kern, Phys. Rev. Lett. **72**, 3378 (1994).
[15] P. Trischberger, H. Dröge, S. Gokhale, J. Henk, H.-P. Steinrück, W. Widdra, and D. Menzel, Surf. Sci. **377-379** 155 (1997).
[16] P. Zeppenfeld, S. Horch, and G. Comsa, Phys. Rev. Lett. **73**, 1259 (1994).
[17] G. Comsa, G. Mechtersheimer, B. Poelsema, and S. Tomoda, Surf. Sci. **89**, 123 (1979).
[18] S. Horch, P. Zeppenfeld, and G. Comsa, Appl. Phys. A **60**, 147 (1995).
[19] J. C. Tully, Surf. Sci. **226**, 461 (1981).
[20] J. M. Gottlieb and L. W. Bruch, Phys. Rev. B **44**, 5750 (1991).
[21] J. E. Black and P. Bopp, Phys. Rev. B **34**, 7410 (1986).
[22] J. E. Black and R. A. Janzen, Phys. Rev. B **39**, 6238 (1989).
[23] J. E. Black and R. A. Janzen, Surf. Sci. **217**, 199 (1989).
[24] C. R. Arumainayagam, R. J. Madix, M. C. McMaster, V. M. Suzawa, and J. C. Tully, Surf. Sci. **226**, 180 (1990).
[25] D. S. Bethune, J. A. Barker, and C. Rettner, J. Chem. Phys. **92**, 6847 (1990).
[26] J. Barker and C. T. Rettner, J. Chem. Phys. **97**, 5844 (1992).
[27] J. E. Müller, Phys. Rev. Lett. **65**, 3021 (1990).
[28] R. A. Aziz and M. J. Slaman, Mol. Phys. **57**, 826 (1986).
[29] J. A. Barker, in *Rare Gas Solids*, edited by M. L. Klein and J. A. Venables (Academic, London, 1976), Vol. 1, p. 212.
[30] L. W. Bruch, Surf. Sci. **125**, 194 (1983), and references therein.
[31] C. Ramseyer, C. Girardet, P. Zeppenfeld, J. Goerge, M. Büchel, and G. Comsa, Surf. Sci. **313**, 251 (1994).
[32] P. Zeppenfeld, M. Büchel, R. David, G. Comsa, C. Ramseyer, and C. Girardet, Phys. Rev. B **50**, 14 667 (1994).
[33] R. Schuster and S. Völkening (unpublished).
[34] S. Picaud, S. Briquez, and C. Girardet, Chem. Phys. Lett. **242**, 212 (1995).